Research Square

Preprints are preliminary reports that have not undergone peer review.
They should not be considered conclusive, used to inform clinical practice,
or referenced by the media as validated information.

Research on optimization of structural parameters of steam pilot solenoid valve based on approximate model

Shuxun Li
Lanzhou University of Technology
Jianlong Zhu
188935308390163.com
Lanzhou University of Technology
Qian Zhao
Lanzhou University of Technology
Wei Li
Lanzhou University of Technology
Zhijun Lei
Lanzhou University of Technology
Bojiang Yin
Lanzhou University of Technology
Jian Zhang
Lanzhou University of Technology

Article

Keywords: Steam-operated solenoid valve, structural parameters, approximate model, quadratic regression model, response surface analysis

Posted Date: September 10th, 2026

DOI: https://doi.org/10.21203/rs.3.rs-10804943/v1

License: This work is licensed under a Creative Commons Attribution 4.0 International License.
Read Full License

Additional Declarations: No competing interests reported.

Research on optimization of structural parameters of steam pilot solenoid valve based on approximate model

Shuxun Li[1,2], Jianlong Zhu[1,2*], Qian Zhao[1,2], Wei Li[1,2], Zhijun Lei[1,2], Bojiang Yin[1,2], Jian Zhang[1,2]

[a] School of Petrochemical Engineering, Lanzhou University of Technology, Lanzhou 730050, PR China

[b] Machinery Industry Pump Special Valve Engineering Research Center, Lanzhou 730050, PR China

[*] Corresponding authors: 18893530839@163.com

Abstract: As a typical precision fluid control component, the opening and closing sensitivity and dynamic response performance of steam-operated solenoid valves have a significant impact on the stability of system operation. Addressing the issue of insufficient response speed in steam-operated solenoid valves, this paper focuses on their overall structural parameters and systematically analyzes the mechanism of their opening and closing response characteristics under static and dynamic conditions. Based on this, using an approximate model method, and with five parameters working air gap, number of coil turns, valve core mass, spring stiffness, and spring preload as optimization variables, quadratic regression models for the pull-in response time and release response time are constructed. Response surface methodology is then used to investigate the interaction between these structural parameters and their impact on dynamic response performance. The results show that each key structural parameter has varying degrees of influence on the pull-in and release response times. Appropriate matching of electromagnetic driving force, moving part inertia, and spring restoring force is crucial for improving the opening and closing performance of the solenoid valve. After optimization, the pull-in response time is reduced to 11.714 ms, and the release response time is reduced to 9.122 ms, significantly improving the dynamic response performance of the solenoid valve. The research results can provide a theoretical basis for the structural optimization and high dynamic response design of steam-operated solenoid valves, and have certain reference value for improving their operational stability and engineering applicability under complex and extreme working conditions.

Keywords: Steam-operated solenoid valve; structural parameters; approximate model; quadratic regression model; response surface analysis

1. Introduction

Facing China's strategy for achieving carbon peak and carbon neutrality, and based

on the practical needs of scientific energy use and efficient energy utilization, industrial steam, as an important driving force for the advancement and modernization of the national industry, has increasingly prominent significance. The clean and low-carbon transformation of industrial steam has become an urgent priority for the industry's development[1]. Therefore, the requirements for the refinement of precision fluid control components have become increasingly stringent, prompting many scholars to conduct extensive systematic research in the field of solenoid valves. In the research of proportional electromagnets, Xie F et al. [2] conducted a systematic analysis of its static and dynamic characteristics based on simulation methods, providing theoretical support for the optimization design of relevant structural parameters. In the research of electromagnetic injectors, Hung N B [3] and Gao H et al. [4] studied the influence of key parameters such as magnetizer height, working air gap width and damping orifice angle on injector performance, revealing the synergistic regulation law of driving current parameters and electromagnetic valve structural characteristics on static electromagnetic performance. Feng Y et al. [5] took the pilot-operated high-speed electromagnetic valve as the research object and studied the influence mechanism of inlet pressure and driving voltage on pressure rise delay time. Wang S et al. [6] used a research method combining numerical simulation and experimental testing to systematically explore the influence of key geometric parameters of proportional electromagnets on their force-displacement characteristics. REN Y et al. [7] innovatively developed a comprehensive modeling method that integrates multi-physics finite element analysis and system dynamics theory. Zhang J et al. [8] used simulation models to analyze in detail the influence of assembly parameters such as residual air gap, spring stiffness and spring preload on the dynamic response characteristics of HSV, and derived the influence law of various structural parameters on its dynamic response characteristics. Cao D et al. [9]proposed a novel parametric equivalent magnetic mesh (EMN) modeling method for multi-objective optimization of surface-mounted permanent magnets. Peng L et al. [10] proposed to optimize the design of high-speed solenoid valves (HSV) and improve their performance by analyzing the electromagnetic force interaction effect between key parameters based on response surface methodology (RSM) through numerical simulation and laboratory experiments.

Since the performance of steam-operated solenoid valves is significantly affected by their structural parameters, optimizing the parameters is crucial for improving performance. In the field of multi-objective optimization of solenoid valves, scholars at home and abroad have achieved many research results. For example, Bhattacharyya B et al. [11] constructed a POD-Kriging model, which uses Proper Orthogonal Decomposition (POD) to predict the response of POD cardinality and performs uncertainty propagation based on the kriging model to help realize the uncertainty quantification of the actual system. Wang et al. [12] trained an SVM surrogate model based on a large amount of data and input this surrogate model into a genetic algorithm to obtain the optimal solution. Peng L et al. [13] proposed two improved structural designs based on the principle of parallel magnetic circuits to improve the performance of high-speed solenoids (HSS) in control systems. In addition, they carried out multi-objective optimization combined with response surface methodology and NSGA-II technology. Yu Z et al. [14] established a simulation model of HSV working process in the high-speed solenoid valve of diesel engine injector and verified it based on armature lift experimental data. By using non-dominated sorting genetic algorithm, HSV multi-objective cooperative optimization under the interaction of dynamic response characteristics and energy loss was completed. Shen D et al. [15] developed an optimization strategy combining BP neural network and optimization genetic algorithm, and screened the best electromagnetic force parameters based on the closeness to the original armature mass. Guo D et al. [16] proposed to use a computationally efficient Dropout neural network to train the surrogate model and innovatively introduced a model management mechanism to coordinate convergence and diversity. This method performed well in solving high-dimensional multi-objective optimization problems. Dong H et al. [17] established a dynamically updated radial basis function surrogate model for each objective and proposed three addition criteria to help complete online sampling in order to achieve a balance between development and exploration. Karidis J P et al. [18] numerically optimized the dynamic performance of electromagnetic actuator-driven switches by combining a hybrid lumped parameter/distributed parameter actuator model with efficient constraint optimization techniques. Feng X et al. [19] proposed a multi-objective optimization for multi-fuel injectors, which reduced

the opening and closing delays by 8.26% and 21.8%, respectively. A collaborative method combining coupling mechanism and NSGA-II optimization is provided for injector design. Chen D C et al. [20] used the maximum magnetic induction intensity as the key optimization index and used the Taguchi method to conduct optimization research on multiple variable parameters. They not only obtained the optimal parameter combination, but also evaluated the influence weight of different factors on the optimization target characteristics. Fan X et al. [21] proposed a multi-physics field collaborative optimization method for actuators. Sensitivity analysis helped to classify design variables into system-level and independent categories. The optimal parameter settings were determined by using a multi-objective genetic algorithm. Meng X et al. [22] used the optimal Latin hypercube test design method in Isight software to analyze the key parameters affecting the oil pressure response characteristics of the proportional solenoid valve, thereby improving the dynamic response characteristics of the proportional solenoid valve. Zhang X [23] and Li T [24] et al. used a combination of finite element simulation and optimal Latin hypercube test design to construct a Kriging proxy model between the solenoid valve structural parameters and electromagnetic force, and used the NSGA-II genetic algorithm to achieve parameter optimization.

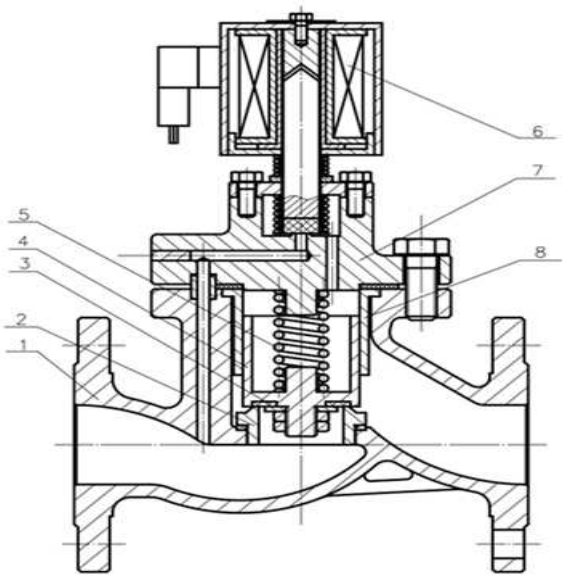
For the aforementioned research, studies and discussions were conducted on the individual performance of the steam pilot-operated solenoid valve, but no systematic research was carried out on the overall structure. This paper addresses the issues caused by the insufficient actuation sensitivity and response speed of the steam pilot-operated solenoid valve, and conducts an optimization study on the overall structural parameters based on an approximate model. Taking the static and dynamic characteristics of the steam pilot-operated solenoid valve as the research foundation, the Box-Behnken design method was employed. The air gap, number of coil turns, valve core mass, spring stiffness, and spring preloading force were selected as optimization targets, and a quadratic regression model for the pull-in response time and release response time was constructed using the response surface method. Response surface analysis was performed on the regression model to obtain the optimal combination of structural parameters to improve the response speed. This study provides an important reference for the system design theory and optimization methods of steam pilot-operated solenoid

valves, with significant theoretical value and engineering application significance.

2. Mathematical model of steam pilot solenoid valve

2.1 Structure and principle of steam pilot solenoid valve

Steam pilot solenoid valve is a normally closed valve, which is mainly composed of valve body, valve seat, sealing ring, valve cup, spring, coil, valve cover, guide sleeve, pilot valve core, etc. When the power is off and in the normal position, the pilot valve port is closed and the main valve is open circuit. When the electrical signal enters the coil of the pilot valve, the movable iron core is moved upward by the electromagnetic force to open the pilot valve port. The internal fluid medium flows to the outlet side through the pilot port. The pressure in the main valve cup drops rapidly. The medium pressure causes the main valve cup to move upward against the force of the spring, realizing the main valve opening and medium circulation. When the signal is interrupted, the moving valve core moves downward due to the reverse force of the spring, closing the pilot valve port, and the fluid at the inlet end enters the inside of the valve cup through the balance hole. When the pressure in the valve cup gradually becomes balanced, the valve cup moves downward under the combined action of the spring force, the self-weight of the valve cup and the medium pressure, and the main valve is in a closed state, cutting off the flow of the medium. The structure of the steam pilot solenoid valve is shown in Fig.1.



1. Valve body 2. Valve seat 3. Seal ring 4. Valve cup 5. Spring 6. Coil 7. Valve cover 8. Guide sleeve

Fig.1. Structural diagram of steam pilot solenoid valve

2.2 Building mathematical models

2.2.1 Electrical subsystem model

The drive circuit of the steam pilot solenoid valve solenoid coil can be simplified into a series circuit of resistance and inductance, and the influence of temperature is ignored. The dynamic differential equation of the circuit is:

$$U = iR_i + \frac{d\psi}{dt} \tag{1}$$

According to the electromagnetic theory, the relationship between the magnetic linkage of the coil, the number of coil turns, magnetic flux, current, and inductance is:

$$\psi = N\phi = Li \tag{2}$$

By converting the flux linkage Ψ in equation (2) with the inductance L, we can get:

$$U = iR_i + \frac{d(L \cdot i)}{dt} = iR_i + i\frac{dL}{dt} + L\frac{di}{dt} \tag{3}$$

In the formula, U is the excitation voltage applied to the coil; i is the coil excitation current; R_i is the internal resistance of the coil; Ψ is the total flux linkage in the coil; N is the total number of turns of the coil; ϕ is the magnetic flux of the coil; L is the coil inductance.

Without considering the core magnetic resistance, eddy current loss and hysteresis effect, the inductance L of the electromagnetic coil is:

$$L = \frac{u_0 N^2 S_0}{h} \tag{4}$$

In the formula, μ_0 is the vacuum magnetic permeability; S_0 is the cross-sectional area of the air gap; h is the length of the air gap.

According to equation (3), the dynamic expression of the coil current is:

$$i = i_0 + \left(\frac{U}{R_i} - i_0\right)\left(1 - \exp(-t\frac{R_i}{L})\right) \tag{5}$$

In the formula, i_0 is the initial current in the coil.

2.2.2 Magnetic subsystem model

In terms of electromagnetic energy conversion of steam pilot solenoid valves, when the coil winding is energized, an excitation magnetic field will be formed around the iron core based on the principle of electromagnetic induction. Magnetic field analysis is generally based on Maxwell's equations, whose differential form is:

$$\begin{cases} \nabla \times H = J \\ \nabla \times E_0 = -\dfrac{\partial B_0}{\partial t} \\ \nabla \times D_0 = \rho_i \\ \nabla \times B_0 = 0 \end{cases} \tag{6}$$

In the formula, ∇ is the Hamilton operator; H is the magnetic field intensity; J is the conduction current density; E_0 is the electric field intensity; B_0 is the magnetic induction intensity; D_0 is the electric flux density; ρ_i is the charge density.

The constitutive relationship between the four field quantities in equation (6) is:

$$\left\{ \begin{array}{l} B = \mu H \\ J = \sigma E_0 \\ D_0 = \varepsilon E_0 \end{array} \right\} \tag{7}$$

In the formula, μ is the magnetic permeability of the soft magnetic material; σ is the electrical conductivity of the soft magnetic material; ε is the dielectric constant.

2.2.3 Mechanical subsystem model

Assuming that the magnetic induction intensity is uniformly distributed on the upper surface of the pilot valve core, the electromagnetic attraction equation of the electromagnet can be obtained according to Kirchhoff's magnetic pressure law and Maxwell's equations:

$$F_e = \frac{1}{2\mu_0} B_0^2 S_0 \tag{8}$$

In the formula, F_e is the electromagnetic force.

At the moment when the steam pilot solenoid valve is opened, the motion equation of the valve core can be obtained from the dynamic motion equation:

$$m\frac{dv}{dt} = F_e - F_k - mg - F_f - F_v \tag{9}$$

In the formula, F_k is the spring force; m is the valve core mass; F_f is the friction resistance of the valve core; F_v is the damping force of the valve core.

The formula for calculating spring force is:

$$F_k = F_0 + kx \tag{10}$$

In the formula, F_0 is the spring preload force; k is the spring elastic coefficient; x is the valve core displacement.

The damping force experienced by the valve core is the viscous resistance generated between the valve core and the medium when it moves. Its calculation

expression is:

$$F_v = cv = c\frac{dx}{dt} \tag{11}$$

In the formula, c is the equivalent viscous damping of the solenoid coil; v is the movement speed of the valve core.

The motion differential equation of the valve core is further obtained as follows:

$$\begin{Bmatrix} \dfrac{dv}{dt} = \dfrac{1}{m}\left[\dfrac{{B_0}^2 S_0}{2\mu_0} - (F_0 + kx) - mg - F_f - cv\right] \\ \dfrac{dx}{dt} = v \end{Bmatrix} \tag{12}$$

2.3 Electromagnet structural parameters

Table 1. Electromagnet key parameter design table

Name	Technical requirements
Pilot valve core radius /mm	7.7
Guide sleeve inner diameter /mm	8
Guide bush thickness /mm	2.5
Skeleton thickness /mm	2
Main air gap width/mm	1
Secondary air gap width/mm	0.3
Coil inner diameter/mm	12.5
Coil outer diameter/mm	24.5
Magnetic body thickness/mm	2.5

Table 1 shows the key parameter design for the electromagnet. Based on these key parameters, we designed and built a model for simulation analysis.

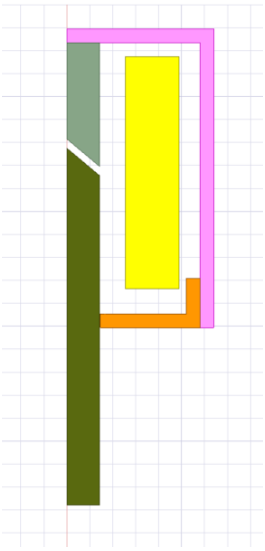
3. Research on static characteristics of steam pilot solenoid valve

3.1 Static characteristics simulation

3.1.1 Construction of simulation model

Maxwell was used to conduct numerical simulation analysis of the static magnetic field characteristics. Based on the actual sizes of the coil, moving iron core, static iron core, etc., a Z-axis two-dimensional rotationally symmetrical proportional model of the steam pilot solenoid valve was established. In order to ensure the accuracy of the simulation calculation and improve the calculation speed, the simulation model was simplified and omitted geometric feature chamfers and fillets that had little impact on

the magnetic circuit analysis. The solenoid valve is a completely axially symmetrical structure and only has a half-section structure. The coil is composed of multiple layers of copper wires, which can be equivalent to a planar structure. The magnetic field distribution of the solenoid valve is relatively concentrated. At the same time, the internal skeleton and guide sleeve of the solenoid pilot valve are all non-magnetic materials, which have little effect on the electromagnetic force. The magnetic permeability of these materials is close to that of air. Therefore, it can be ignored during modeling and only the magnetic components and coils of the magnetic circuit are simulated and modeled. The model is shown in Fig.2 below, and it is meshed, as shown in Fig.3 below.



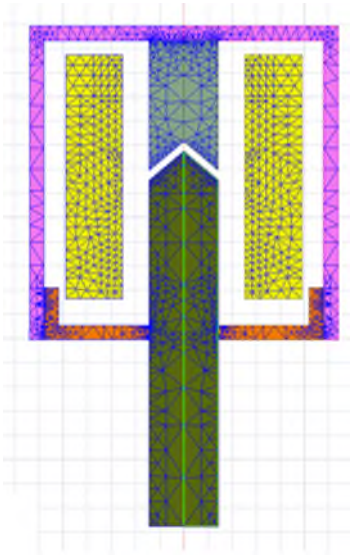


Figure.2. Two-dimensional finite element model **Figure.3.** Two-dimensional model meshing

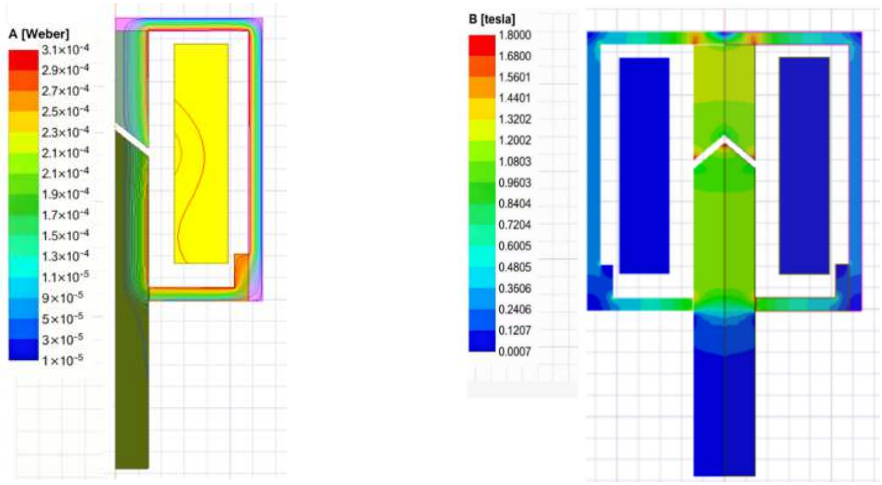
3.1.2 Material definition

The selection of magnetic circuit materials for steam pilot-operated solenoid valves primarily involves choosing materials for key components such as the fixed iron core, movable iron core, and electromagnetic coil. Since the movable iron core valve stem is isolated from the steam at the lower end, the medium between the movable iron core and the electromagnetic coil is air. In electromagnetic simulations, the air domain is typically modeled as either a vacuum or air medium, with its relative magnetic permeability set to 1. For the coil winding portion, commonly used soft magnetic materials include low carbon steel, DT4C, and 430 magnetic steel. During the simulation process, the permeability corresponding to any magnetic field strength is

obtained by defining the B-H magnetization curves for each material. Since the electromagnetic parameters of copper conductors are already built into the material library of finite element analysis software, standard copper material parameters can be directly used for modeling. The relative magnetic permeability of copper wire is 1, and its electrical conductivity is 5.8×10^{7}S/m.

3.1.3 Simulation result analysis

Based on the constructed finite element simulation model of the magnetic field, when the coil excitation current is set to 0.44A and the air gap between the dynamic and static cores is 2mm, the magnetic field lines and magnetic induction intensity distribution of the solenoid valve are shown in Fig.4 The simulation results show that the magnetic lines of force generated by the energized coil are mainly concentrated in the magnetic conductive loop composed of soft magnetic materials, and this path forms a complete closed loop of magnetic flux. It can be seen from the magnetic field cloud diagram in the figure that there is a high magnetic induction intensity distribution characteristic at the top of the moving iron and the bottom of the static iron. This magnetic field concentration effect can effectively enhance the electromagnetic attraction and ensure the ideal action response of the solenoid valve.



(a) Magnetic field line distribution cloud (b) Magnetic susceptibility intensity cloud

Fig.4. Magnetic field simulation cloud diagram

After completing the finite element modeling and simulation analysis, the following key calculation results can be obtained to evaluate the performance characteristics, as shown in the electromagnetic force-displacement characteristic curve in Fig.5. As the displacement increases, the electromagnetic force also increases

because as the valve core moves, the magnetic circuit gradually closes, the magnetic resistance decreases, and the electromagnetic force increases. The peak point of the curve corresponds to the maximum value of the electromagnetic force, when the solenoid valve is most efficient.

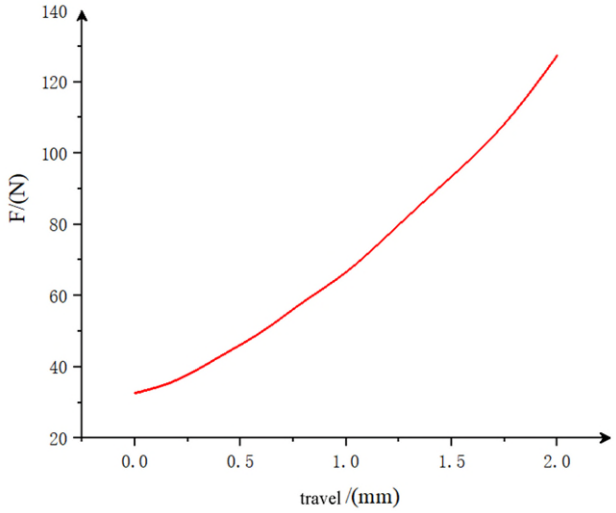


Fig.5. Solenoid valve force-displacement characteristic curve

3.2 Analysis of factors affecting electromagnetic characteristics

3.2.1 Influence of working air gap

Based on the established geometric model, the electromagnetic force characteristics under different working air gap conditions were simulated and analyzed. The changes in the electromagnetic force when the air gap changes from 1.6mm to 2.2mm are shown in Fig.6. The simulation results show that under the condition that the excitation current remains constant, the electromagnetic force has a negative correlation with the working air gap, that is, as the air gap increases, the electromagnetic force gradually decreases. This phenomenon occurs because as the height of the working air gap increases, the volume of the air domain through which the magnetic field needs to flow increases, the air gap magnetic resistance increases, and the magnetic induction intensity decreases, thus causing the electromagnetic force to decrease, and the reduction rate of the electromagnetic force is affected by the size of the current, so the length of the air gap should be reduced if allowed.

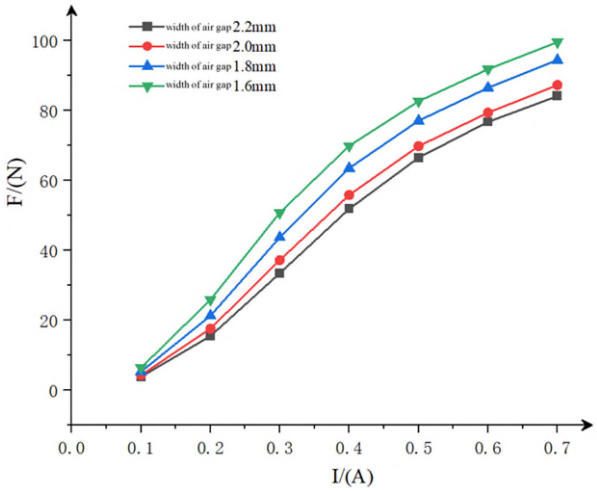


Fig.6. Effect of working air gap on electromagnetic force

In addition, the study also found that there is a significant correlation between the size of the working air gap and the sensitivity of the electromagnetic force-current characteristics. When the air gap is small, the response of the electromagnetic force to the current change is more significant. When the air gap decreases from 2.2mm to 2.0mm, the increase in the electromagnetic force is relatively slow, which indicates the nonlinear characteristics of the electromagnetic force as the air gap changes. Therefore, the working air gap parameters need to be comprehensively selected based on the actual situation.

3.2.2 Effect of coil turns

Based on the established simulation model, the static characteristics of the solenoid valve under different number of turns conditions were simulated and analyzed, and the comprehensive effect of different numbers of coil turns and input current on the electromagnetic force of the solenoid valve when the working air gap was 2mm was studied. The results are shown in Fig.7.

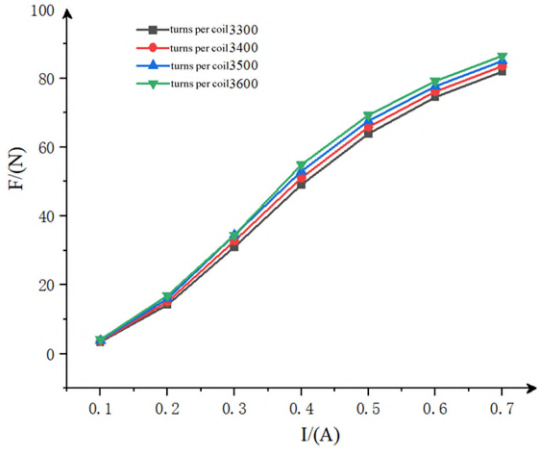


Fig.7. Effect of coil turns on electromagnetic force

The simulation results show that under the condition that the current and the working air gap are the same, when the number of coil turns increases from 3300 to 3600, the electromagnetic driving force generated increases, and there is a positive correlation between the size of the electromagnetic force and the number of coil turns. However, increasing the number of coil turns is not always beneficial under actual operating conditions, because too many turns will lead to an increase in inductance, which will slow down the current rise rate, reduce the dynamic response speed of the electromagnetic force, and affect the transient performance of the solenoid valve.

3.3 Literature verification

Due to limitations the experimental prototype of the steam-operated solenoid valve was not processed, and the experiment needs to be completed later. Therefore, based on extensive literature review, the static characteristic analysis of the solenoid valve was verified by literature. Reference [25] analyzed the influence of working air gap, number of coil turns, ratio of attraction area and valve core magnetic material on electromagnetic characteristics. The simulation results showed that under a certain current, the electromagnetic force decreased with the increase of air gap and increased with the increase of number of coil turns. Reference [26] studied the influence of number of coil turns, outer diameter of main magnetic pole, thickness of armature, excitation current and working air gap on static electromagnetic force, showing that the electromagnetic force increased with the increase of number of coil turns. Comparing the simulation results of the above literature with the simulation results in this section, it is shown that the law obtained by static characteristic simulation is consistent with the law obtained by the above literature simulation.

4. Research on dynamic characteristics of steam pilot solenoid valve

4.1 Establishment of dynamic model of steam pilot solenoid valve

4.1.1 Dynamic model equations

Establish its dynamic equation based on the opening process of the main valve cup:

$$Ma = F_g + F_{k1} + F_{f1} - F_p \tag{13}$$

In the formula, M is the mass of the main valve cup; a is the acceleration of the main valve cup; F_{k1} is the spring force on the main valve cup; F_{f1} is the friction force on the main valve cup; $F_p=P_1A_1-P_2A_2$, is the gas force on the valve core; P_1 is the

pressure on the lower end of the main valve cup; P_2 is the pressure on the upper end of the main valve cup; A_1 is the flow cross-sectional area of the main valve; $A_2$is the flow area of the control chamber.

Assuming that the movement stroke of the main valve core is x_1, the fully opening time T_z of the main valve core can be expressed as:

$$T_Z = \sqrt{\frac{2x_1}{a}} = \sqrt{\frac{2x_1 M}{F_g + F_{k1} + F_{f1} - P_1 A_1 + P_2 A_2}} \tag{14}$$

From equation (14) that although the force situation during the movement of the main valve cup is relatively complex, the opening time is mainly affected by the movement stroke x_1.

The opening process of the steam pilot solenoid valve is very short. It can be approximately considered that the thermodynamic changes between the chambers follow isentropic conditions. Under this assumption, the relationship between the pressure in the main valve chamber and the change with time is:

$$\frac{dP_1}{dt} = \frac{kR(T_0 Q_{m0} - T_1 Q_{m1}) - kP_1 A_1 dx/dt}{V_1 + A_1 x} \tag{15}$$

The pressure change equation of the control chamber during the exhaust stage can be expressed as:

$$\frac{dP_2}{dt} = \frac{-kRT_2 Q_{m2} + A_2 kP_2 dx/dt}{V_2 + A_2 x} \tag{16}$$

In the formula, k is the adiabatic index of steam, 1.33; R is the gas constant for steam, taken as 461.5 J/(mol·k); T_0 is the gas thermodynamic temperature at the inlet of the main valve cavity; Q_{m0} is the main valve inlet gas mass flow rate; T_1 is the gas thermodynamic temperature at the main valve exhaust port; Q_{m1} is the main valve exhaust gas mass flow rate; $V_1$is the main valve cavity volume; T_2 is the exhaust temperature of the control chamber; V_2 is the volume of the control chamber.

4.1.2 Dynamic response characteristics simulation

A numerical simulation model of dynamic response characteristics was established in the Matlab/Simulink simulation environment. The simulation model is established through the mathematical model of the circuit module, as shown in Fig.8.

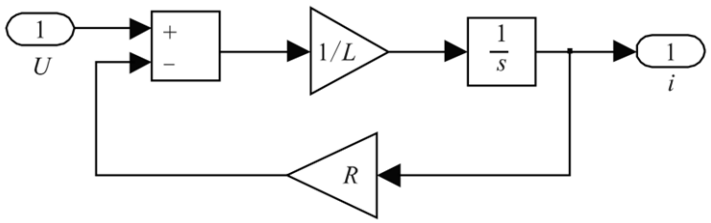


Fig.8. Circuit module simulation model

According to the formula, the simulation model of the magnetic circuit module can be established, as shown in Fig.9. The input variables of this model come from the output parameter *i* of the circuit simulation model, and the output parameter of the magnetic circuit model is the electromagnetic force *F*.

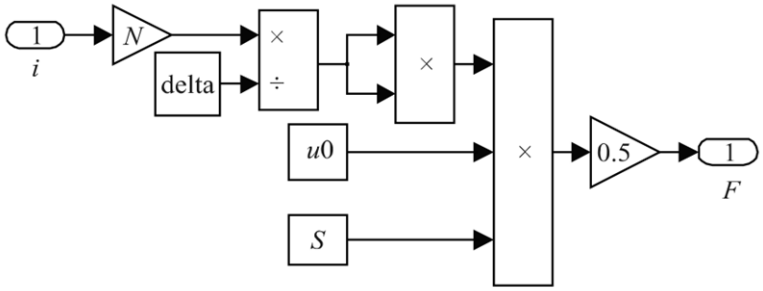


Fig.9. Magnetic circuit module simulation model

The simulation model of the motion module is established according to the formula, as shown in Fig.10. The input of the motion module simulation model is the electromagnetic force *F*, and the output parameters are the armature's motion speed *V* and motion displacement *X*.

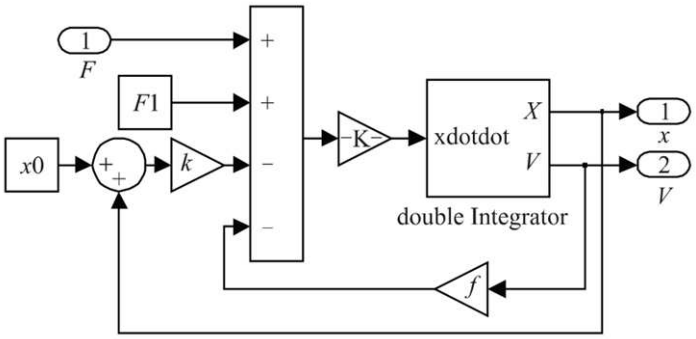


Fig.10. Motion module simulation model

Fig.11 shows the integrated simulation model of dynamic characteristics, which is formed by combining the simulation models of the three subsystems of circuit, magnetic circuit and mechanical motion. The figure shows the parameter input and output connections between the three models.

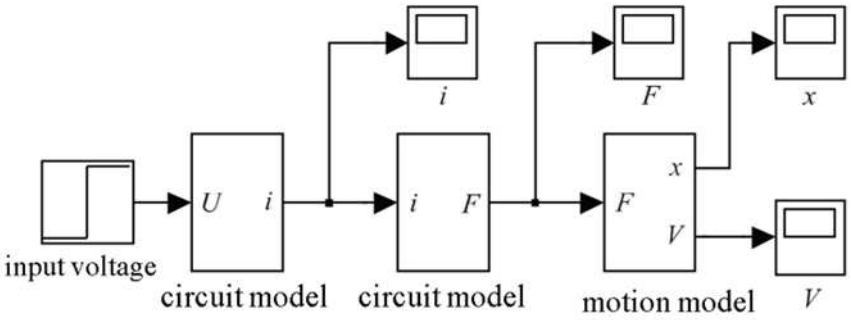


Fig.11. Solenoid valve dynamic characteristics simulation model

4.1.3 Simulation results

The results of the displacement response simulation curve are shown in Fig. 12. The curve completely presents the motion characteristics of the steam pilot solenoid valve during the opening and closing process, and can intuitively reflect its dynamic response performance. From Fig.12, it can be seen that when the input signal is applied, the valve core starts to move, but because it takes time to establish inertia and electromagnetic force, there will be a delay in the displacement response.

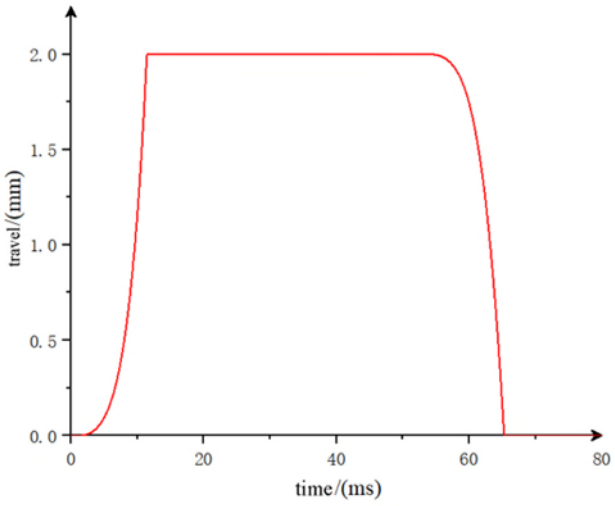


Fig.12. Displacement response simulation curve

4.2 Analysis of influencing factors on dynamic response of steam pilot solenoid valve

4.2.1 Influence of valve core quality

As a key physical characteristic of moving parts, the valve core quality directly affects the dynamic performance of the steam pilot solenoid valve. Fig.13 shows the valve core displacement-time response curve when the valve core mass m is 94g, 96g, 98g, and 100g respectively. The simulation results show that when the valve core mass

increases, the opening and closing times of the valve core are lengthened accordingly. Therefore, optimizing the response speed of the valve core requires appropriately reducing its quality. However, this improvement measure brings two problems at the same time: First, the material needs to be lightweight while ensuring mechanical strength and durability, which may increase manufacturing costs; second, too small a mass may make it difficult to control processing accuracy.

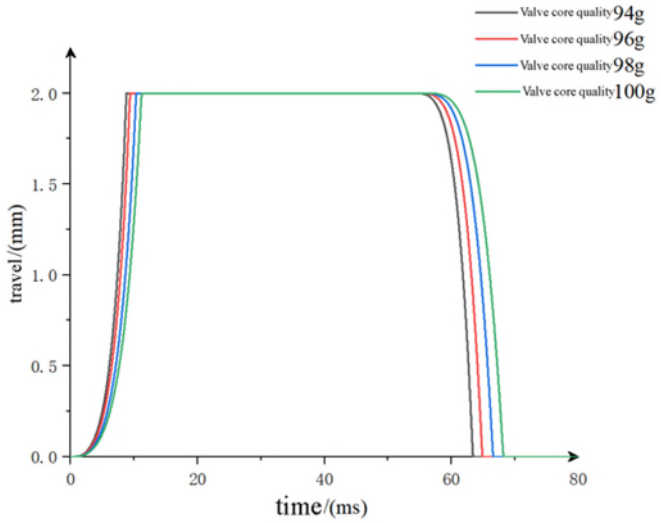


Fig.13. Effect of valve core quality on displacement-time response

4.2.2 Effect of spring stiffness

Changes in spring stiffness have a significant impact on the dynamic response time of the steam pilot solenoid valve, as shown in the simulation results in Figure 14. In steam pilot solenoid valves, the spring stiffness directly affects the movement characteristics of the valve core, showing different rules during the opening and closing stages. During the opening process of the solenoid valve, since the steam pilot solenoid valve has a normally closed structure, the spring force acts as a resistance that hinders the movement of the moving iron core. Therefore, the greater the stiffness, the longer the opening response time of the moving iron core. In the closing stage, the spring force is converted into the power to drive the valve core to reset, and the increase in stiffness will significantly shorten the closing time of the moving iron core. However, the increase in spring stiffness is not unlimited. Excessive stiffness may cause the valve core to fail to reach the rated stroke, thus affecting the normal operation of the solenoid valve.

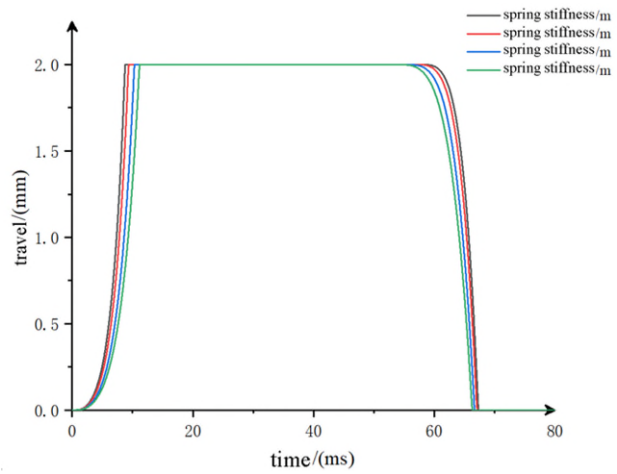


Fig.14. Effect of spring stiffness on the opening response of the solenoid pilot valve

4.2.3 Effect of spring preload

The dynamic response characteristics of the steam pilot solenoid valve are dually affected by spring preload force and spring stiffness, and the effects of the two show opposite trends. Among them, the spring preload force not only affects the opening process of the valve body, but also significantly affects its closing process. As shown in Fig.15, during the pull-in phase of the moving iron core, the spring preload force appears as a force that hinders the movement of the iron core; while during the reset phase, this force is converted into power to drive the iron core back, prompting the valve core to move downward and complete the closing of the solenoid valve. The simulation results show that increasing the spring preload force will prolong the pull-in time of the moving iron core, but at the same time shorten the reset time.

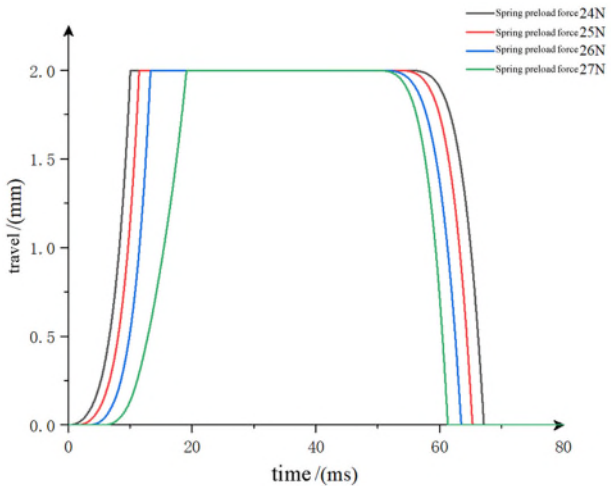


Fig.15. Effect of spring preload on displacement-time response

4.3 Literature verification

Due to limitations, the experimental prototype of the steam pilot solenoid valve

was not processed, and the experiment needs to be completed later. Therefore, based on extensive literature review, the dynamic response characteristics of the solenoid valve were verified by literature. Reference [27] studied the influence of variables such as valve core mass, driving voltage, number of coil turns, and initial air gap on the dynamic response of the solenoid valve. The results showed that during the opening and closing stages of the solenoid valve, the greater the valve core mass, the longer the valve core opening and closing time. Reference [28] studied the influence of variables such as spring stiffness, moving component mass, and excitation voltage on the dynamic response of the solenoid valve. It concluded that the greater the spring stiffness, the slower the solenoid valve's pull-in response time and the faster the reset response time. Reference [29] analyzed the influence of spring preload, working air gap, spring elastic coefficient, armature fine diameter, excitation voltage, and number of coil turns on the opening response time of the solenoid valve through a dynamic simulation model. It concluded that the greater the spring preload, the longer the time required for the moving iron core to pull in, but the shorter the iron core reset time. Comparing the simulation results from the above literature with those from this section shows that the patterns derived from the dynamic characteristic simulation are consistent with those derived from the above literature simulation.

5. Research on optimization of structural parameters of steam pilot solenoid valve

5.1 Multi-objective optimization based on approximate model

5.1.1 Approximate model and experimental design

The essence of typical engineering design problems is multi-objective, requiring the simultaneous optimization of multiple objectives while satisfying various constraints. Optimization problems that involve multiple objectives are referred to as multi-objective optimization problems. Compared with traditional optimization methods, this algorithm imposes more relaxed constraints on the objective functions and is particularly suitable for solving the Pareto optimal frontier. This advantage has led to its widespread application in the field of engineering optimization [30].

Approximate model technology is a modeling method that uses mathematical methods to construct an approximate relationship between input and output variables.

In the field of multi-objective optimization design, common agent models are mainly divided into three categories: Radial Basis Function Model, Kriging Model, and Polynomial Response Surface Model, etc.[31]

Based on the multi-objective optimization framework, this paper adopts the modeling method of polynomial response surface model and carries out the experimental design at the first step. The experimental design adopts the Box-Behnken design method. Its advantage is that it takes into account the random error of the experiment and can use fewer experimental plans to obtain the optimal combination of structural parameters. The specific experimental design is shown in Table 2. Each optimization parameter has three levels. Each optimization parameter is coded -1, 0, and 1, where 0 is the center point of the optimization variable, 1 is the maximum value, and -1 is the minimum value. The experimental results are shown in Table 3, with a total of 46 experiments of 5 factors and 3 levels.

Table 2. Test coding levels

parameter	element	level		
		low	medium	high
working air gap	*A*	-1	0	1
Coil turns	*B*	-1	0	1
Valve core qualit	*C*	-1	0	1
spring stiffness	*D*	-1	0	1
spring preload	*E*	-1	0	1

Table 3. Test results

Standard Order	Run Order	*A* working air gap	*B* Coil turns	*C* Valve core qualit	*D* spring stiffness	*E* spring preload force	R_1	R_2
19	1	2	3400	98	500	26	17.66	13.95
41	2	1.6	3600	98	500	26	18.22	14.41
…	…	…	…	…	…	…	…	…
35	45	1.6	3400	98	500	24	11.33	16.52
8	46	2	3400	98	700	24	12.9	8.09

5.1.2 Anova and regression model diagnostics

Import the simulation results into Design-Expert, fit a regression model based on the simulation data, and establish the quadratic regression model equations of the pull-in response time R_1 and the release response time R_2 respectively. The quadratic

regression equations of R_1 and R_2 are as shown in equations (17) and (18), which describe the relationship between the independent variables and the response variables.

$$\begin{aligned} R_1 &= 18.18 + 0.9125A - 1.57B + 0.8319C - 1.27D + 0.3106E + 0.8050AB \\ &-0.4650AC - 0.6600AD - 0.0100AE + 0.5225BC - 0.1750BD + 1.58BE \\ &-2.67CD - 0.5150CE - 1.23DE - 3.44A^2 - 2.78B^2 - 3.40C^2 - 2.3D^2 - 2.86E^2 \end{aligned} \quad (17)$$

$$\begin{aligned} R_2 &= 13.96 + 1.54A - 0.4775B + 0.7694C - 0.4319D + 0.2400E + 1.56AB \\ &-0.7150AC - 0.1600AD + 0.4900AE - 0.4775BC - 0.3250BD + 2.30BE \\ &-1.93CD - 0.7650CE - 0.9775DE - 3.14A^2 - 2.69B^2 - 3.86C^2 - 3.05D^2 - 3.30E^2 \end{aligned} \quad (18)$$

The results of the analysis of variance of the pull-in response time R_1 and the release response time R_2 are shown in Tables 4 and 5. After the model is established, analysis of variance ANOVA is used to evaluate the overall significance of the model.

Table 4. R_1 variance analysis results

source	sum of squares	mean square value	Statistical test value F value	Probability P value	Significance
Model	336.74	16.84	41.28	<0.0001	Extremely significant
A working air gap	13.32	13.32	32.67	<0.0001	Extremely significant
…	…	…	…	…	…
E^2	71.36	71.36	174.98	<0.0001	Extremely significant
Lack of Fit	9.54	0.4770	3.64	0.0784	Not significant

Table 5. R_2 variance analysis results

source	sum of squares	mean square value	Statistical test value F value	Probability P value	Significance
Model	334.60	16.73	86.97	<0.0001	Extremely significant
A working air gap	37.82	37.82	196.61	<0.0001	Extremely significant
…	…	…	…	…	…
E^2	95.08	95.08	494.24	<0.0001	Extremely significant
Lack of Fit	4.46	0.2229	3.17	0.1019	Not significant

As the probability P value decreases and the test statistic F value increases, the input parameters have a more significant impact on the response. Set the confidence interval to 95%. When the P value is less than 0.05, it means that the factor has a significant impact. When the P value is less than 0.0001, it means that the factor has an

extremely significant impact. As can be seen from Tables 4 and 5, the F values of the standard quadratic regression models of R_1 and R_2 are 41.28 and 86.97 respectively, and the P values are both less than 0.0001. The multiple correlation coefficient is a commonly used measure for testing prediction models and is used to compare the degree of matching between the prediction results and the actual situation. R_1, the coefficients of determination of the R_2 model are 0.9706 and 0.9858 respectively, which shows that the consistency between the predicted value based on the response surface and the real value is very strong. It also shows that the response surface model has reached an extremely significant level and the fitting accuracy is good. The response surface model can be used for subsequent prediction and optimization design of R_1 and R_2. In addition, the applicability and significance of the model are tested through various statistical factors in the table. The coefficient of variation is the ratio of the standard deviation to the mean, and is a normalized measure that reflects the degree of dispersion of the model. The coefficients of variation of the R_1 and R_2 quadratic regression models in the study were 1.93% and 0.526% respectively, indicating that the model has high accuracy. According to the analysis results, it can be seen that the significance of the two models is relatively high.

5.2 Response surface analysis

It can be seen from the variance analysis results of R_1 and R_2 that the interaction of each factor affects the order of R_1 and R_2. By analyzing the results obtained from different parameters, the response surface plot and contour plot can be obtained from the quadratic response surface regression model.

As shown in Fig.16, the response surface of the interaction of spring stiffness and valve core mass on R_1 when A, B, and E are at the horizontal intermediate value. When the spring stiffness is at a low level, the value of R_1 will increase sharply as the mass of the valve core increases. After the valve core mass is about 100g, it tends to level off. When the spring height is at a high level, as the valve core mass increases, R_1 will first increase and then decrease and the decrease will be greater than the increase. When the valve core mass is at a high level, as the spring stiffness increases, the value of R_1 will gradually decrease. When the valve core mass is at a low level, as the spring stiffness increases, R_1 will first increase and then decrease slightly. The response surface is tilted

toward the D-axis greater than the C-axis. According to the contour plot, it can be seen that the curve density of the D-axis will be greater than the curve density of the C-axis, which is consistent with the results of variance analysis. At the same time, the interactive response surface of the spool mass and spring stiffness is the steepest set of all surfaces and the most significant set.

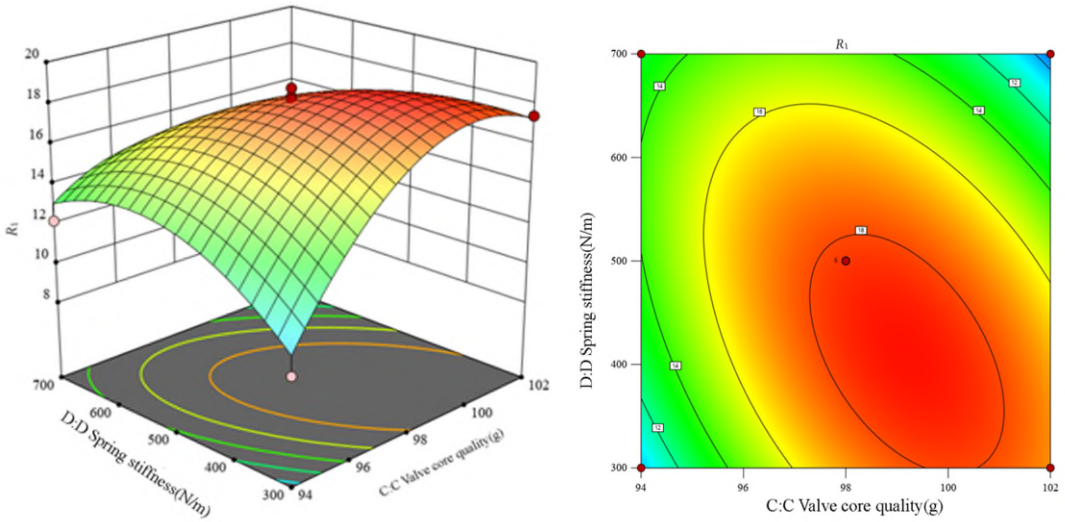


Fig.16. Response surface of spring stiffness and valve core mass to R_1

Fig.17 is the response surface of the influence of the number of coil turns and spring preload on R_1 when *A, C*, and *D* are at the horizontal intermediate value. No matter when the spring changes in any horizontal value, as the number of coil turns increases, the value of R_1 will first increase slightly and then decrease significantly. As the spring preload force increases, the rise in R_1 becomes larger as the number of coil turns increases in the early stage. When the number of coil turns is at a high level, as the spring preload force decreases, the value of R_1 will first increase slightly and then decrease significantly. The inclination of the curved surface is more inclined to the B-axis coil turns. At the same time, according to the analysis of the contour diagram, the density of the curve intersecting the B-axis will be greater than the E-axis. In line with the variance analysis, the significance of the number of coil turns is greater than the significance of the spring preload.

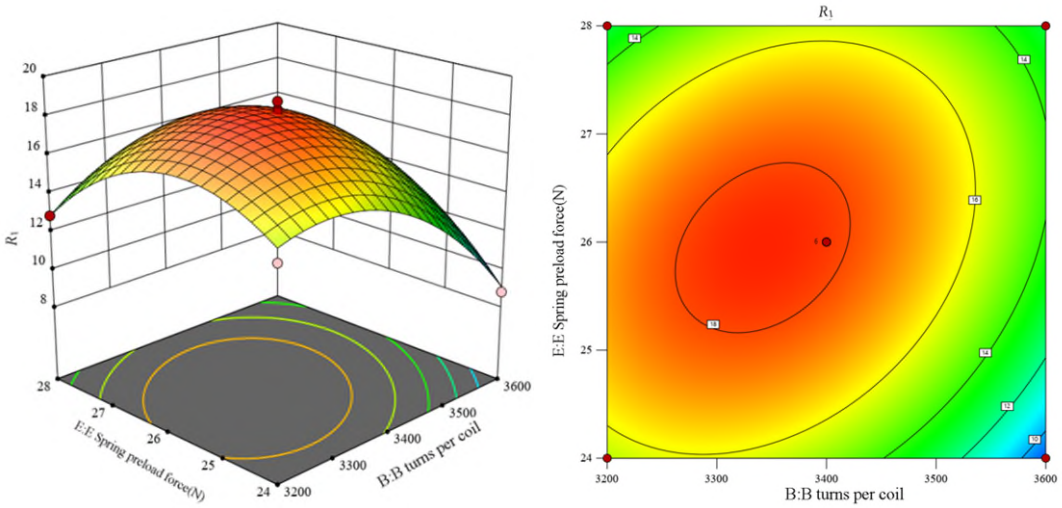


Fig.17. Response surface of coil turns and spring preload force to R_1

Fig.18 is the response surface of the interaction of spring stiffness and spring preload force on R_1 when A, B, and C are at the horizontal intermediate value. When the spring preload is at a low level, R_1 will first increase and then decrease as the spring stiffness increases. When the spring preload force is at a low level, as the spring stiffness increases, R_1 will increase slightly and then drop sharply. When the spring stiffness is at a low level, R_1 will gradually increase and finally decrease slightly as the spring preload force increases. When the spring stiffness is at a high level, R_1 increases slightly and then suddenly decreases as the spring preload force increases. The density of the curve where the contour line intersects the D-axis is greater than the curve density of the E-axis.

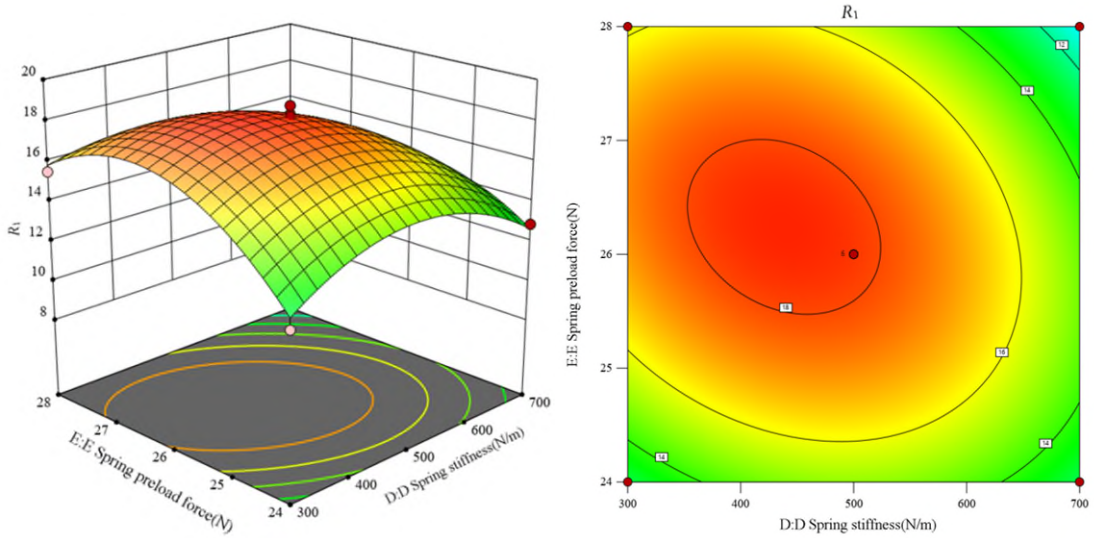


Fig.18. Response surface of spring stiffness and spring preload force to R_1

Fig.19 is the response surface of the interaction of the working air gap and the

number of coil turns on R_1 when C, D, and E are at the horizontal intermediate value. No matter the number of coil turns changes at any level, the R_1 value will first increase and then decrease as the working air gap increases. However, the overall response value changes more at the low level of coil turns than at the high level. And the highest point is generated between the two levels. The density of the curves that intersect the B-axis in the contour plot is greater than the density of the curves that intersect the A-axis.

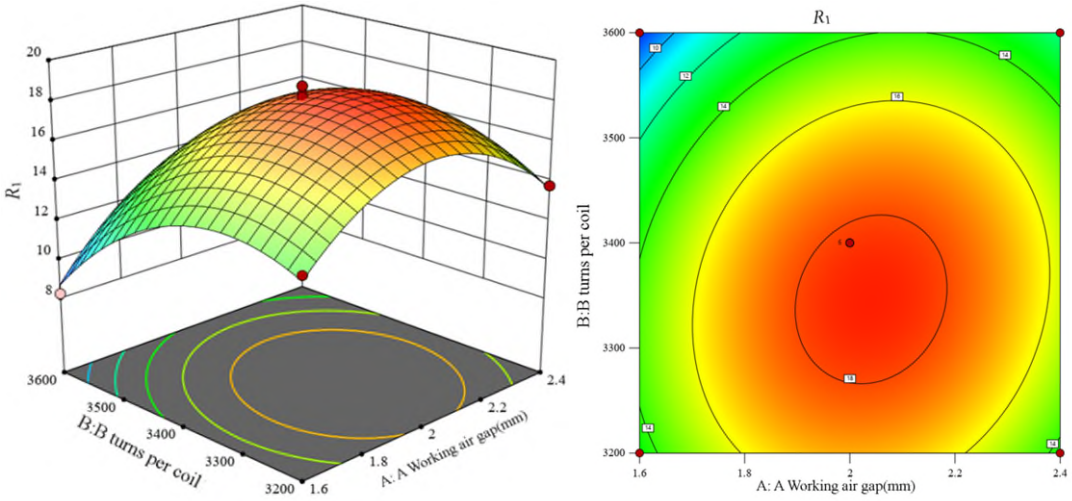


Fig.19. Response surface of working air gap and coil turns to R_1

Fig.20 is the response surface of the interaction of the working air gap and spring stiffness on R_1 when B, C, and E are at intermediate level values. When the spring stiffness is at a low level, R_1 first increases and then decreases slightly as the working air gap increases. In the contour plot, the density of the curve that intersects the D-axis is greater than the density of the curve that intersects the A-axis.

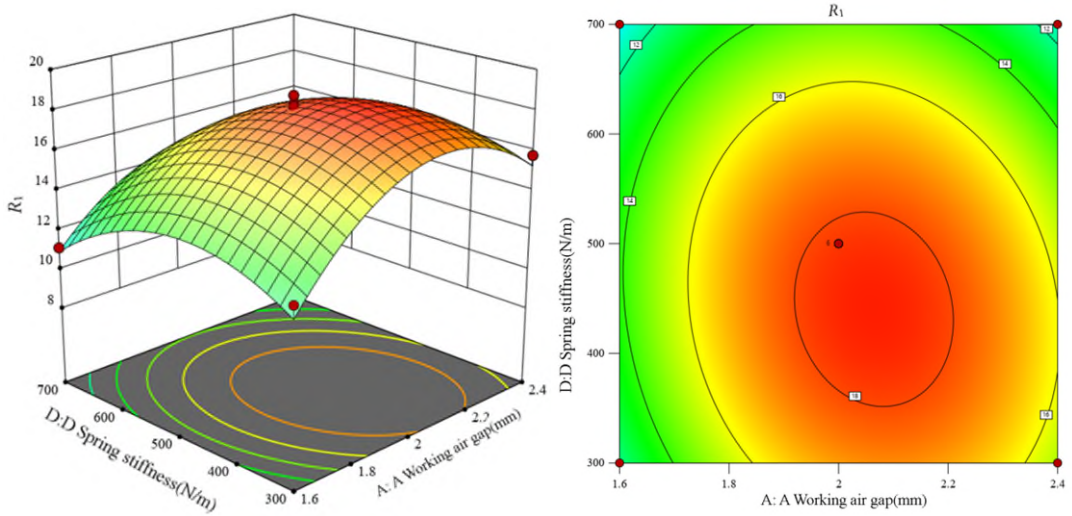


Fig.20. Response surface of working air gap and spring stiffness to R_1

Fig.21 is the response surface of the interactive influence of coil turns and spring preload on R_2 when A, C, and D are at intermediate level values. When the spring preload force is at a low level, R_2 will increase slightly and then decrease suddenly as the number of coil turns increases. When the spring preload is at a high level, R_2 will rise sharply and then slowly decrease as the number of coil turns increases. The response surface is more inclined to the B-axis, and the density of the curves in the contour plot that intersects the B-axis is greater than the density of the curves that intersect the E-axis.

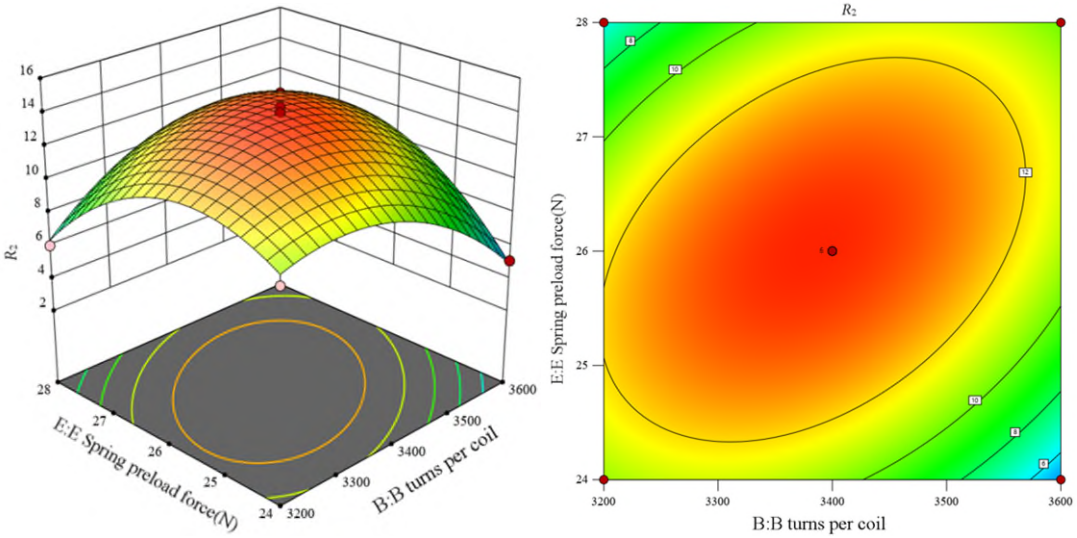


Fig.21. Response surface of coil turns and spring preload force to R_2

Fig.22 is the response surface of the interaction of the valve core mass and spring stiffness on R_2 when A, B, and E are at intermediate levels. Regardless of the spring stiffness at any level, R_2 will first increase and then decrease as the valve core mass increases, but at a low level, R_2 rises sharply as the valve core mass increases. The slope of the response surface is closer to the C-axis, and the density of the curves relative to the C-axis in the contour plot is also greater than the D-axis.

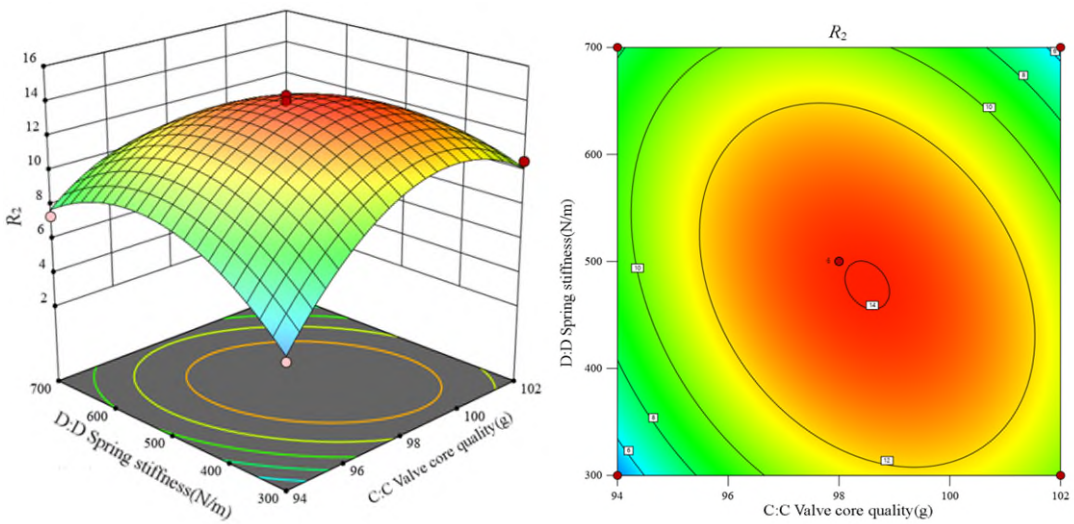


Fig.22. Response surface of R_2 for spool mass and spring stiffness

Fig.23 is the response surface of the interaction of the working air gap and the number of coil turns on R_2 when C, D, and E are at intermediate levels. As the working air gap increases, the value of R_2 will first rise and then decrease. However, when the number of coil turns is low, the increase in the working air gap will cause R_2 to rise and then slowly decrease. At the same time, the density of the curve intersecting the working air gap of the A-axis in the contour diagram is greater than that of the B-axis.

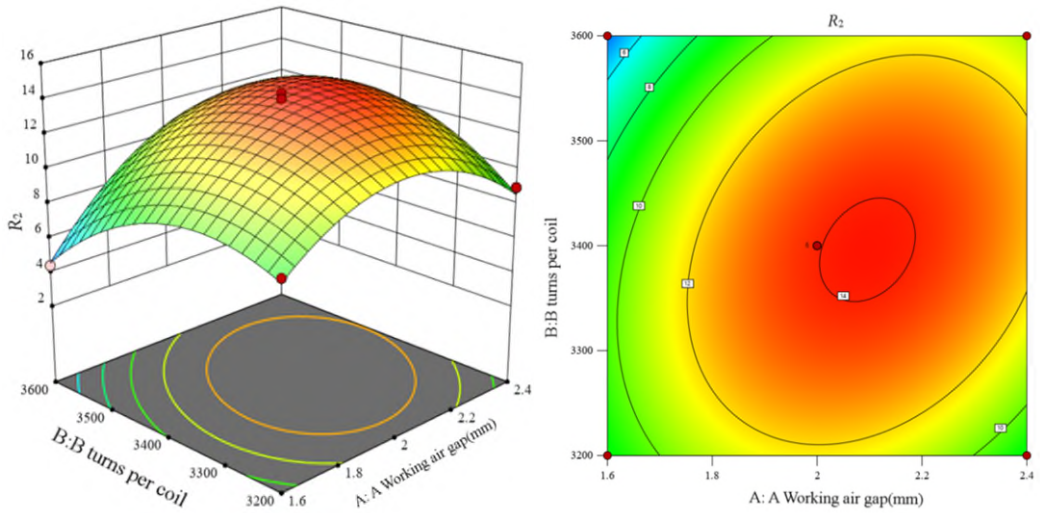


Fig.23. Response surface of working air gap and number of coil turns to R_2

Fig.24 is the response surface of the interactive influence of spring stiffness and spring preload force on R_2 when A, B, and C are at the intermediate level value. No matter the spring preload is at any level, R_2 will first rise and then decrease as the spring stiffness increases. The difference is that R_2 rises sharply when the spring preload is in a horizontal position. As the spring stiffness and preload force continue to increase, the

impact on the R_2 value also increases first and then decreases. The highest point of the response value is at the horizontal middle of the spring stiffness and spring preload force. At the same time, the density of the curve that intersects the B-axis in the contour diagram is greater than the curve density of the E-axis.

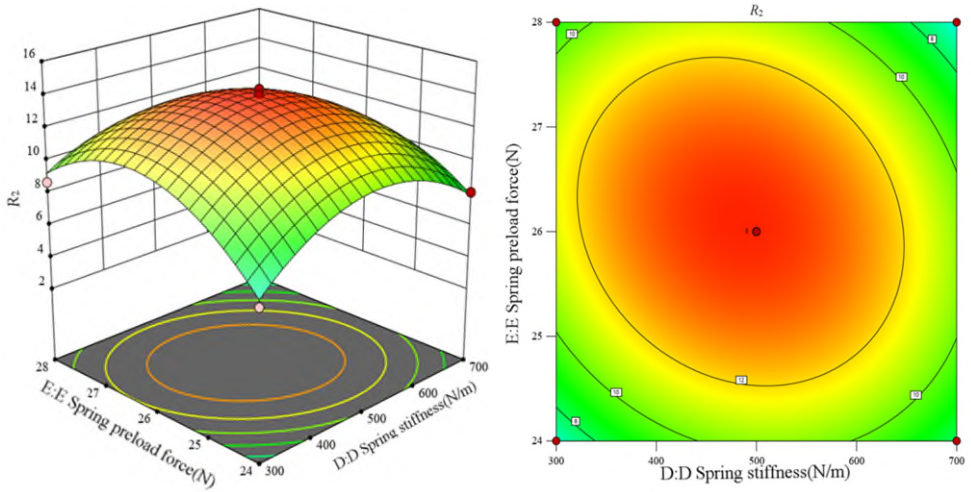


Fig.24. Response surface of spring stiffness and spring preload force to R_2

Fig.25 is the response surface of the interaction of the valve core mass and the spring preload force on R_2 when A, B, and D are at intermediate levels. As the quality of the valve core increases, the R_2 value will first increase and then decrease, but when the spring preload level is low, R_2 rises sharply. As the spring preload force increases, the R_2 value will first increase and then decrease. When the valve core quality level is low, as the spring preload force increases, R_2 will increase slightly but then decrease suddenly. At the same time, the density of the curve that intersects the C-axis in the contour plot is greater than the E-axis.

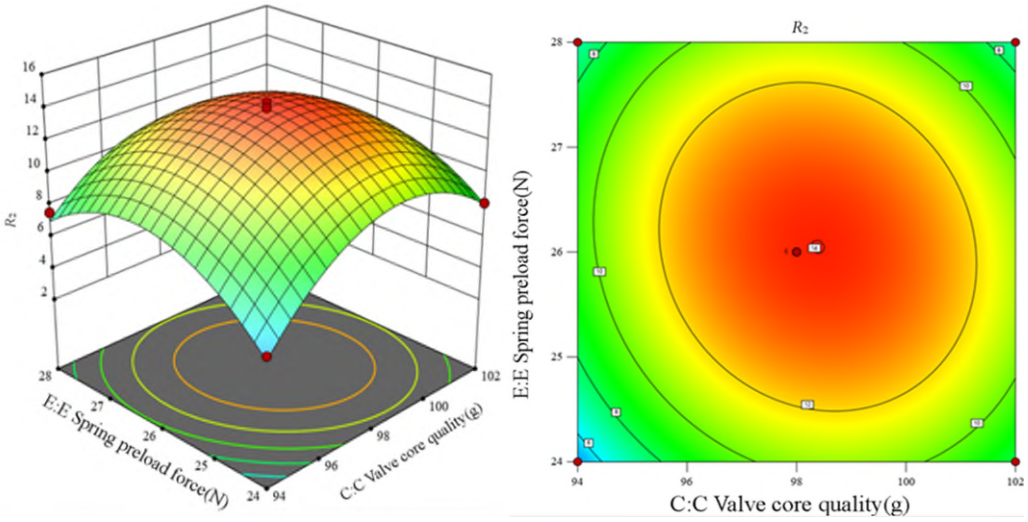


Fig.25. Response surface of valve core mass and spring preload force to R_2

5.3 Analysis of optimization results

Combining surrogate modeling techniques with experimental design methods, regression model equations for pull-in response time and release response time were established, and the accuracy of the models was verified using variance analysis and residual analysis. The results all showed that the regression model equations for pull-in response time and release response time were highly accurate. Using the regression models, multi-objective optimization was carried out for pull-in response time and release response time. Response surface analysis results indicated that the interactions between different factors of pull-in response time and release response time all showed good linear relationships. The optimal solenoid valve structure parameters were finally determined as: *A* working air gap 2.1mm, *B* coil turns 3375, *C* valve core mass 99g, *D* spring stiffness 450N/m, *E* spring preload 26N. By inputting the optimal parameters into the dynamic characteristic simulation model, the response time was improved, resulting in a solenoid valve pull-in response time R_1 of 11.714ms and release response time R_2 of 9.122ms.

6. Conclusion

This paper addresses the shortcomings in the sensitivity and response speed of steam-operated solenoid valves. Taking its overall structural parameters as the research object, it systematically analyzes the mechanism of the opening and closing response characteristics of steam-operated solenoid valves under static and dynamic characteristics. Based on this, the interaction between various structural parameters and their impact on response performance are studied using an approximate model method, and the structural parameters are optimized.

(1) Based on the working characteristics of the steam-operated solenoid valve, a magnetic circuit model, a circuit model, and a motion model are established, providing a theoretical basis for the static and dynamic simulation analysis of the steam-operated solenoid valve. Using Maxwell finite element simulation software, the static characteristics simulation analysis of the steam-operated solenoid valve is carried out. The influence of the working air gap and the number of coil turns on the electromagnetic force is analyzed, and the influence law of electromagnetic characteristics is obtained: when the working air gap increases, the electromagnetic

force decreases, and the magnitude of the decrease gradually increases. Simultaneously, the electromagnetic force increases with the increase of the number of coil turns.

(2) The dynamic characteristics of the designed steam-operated solenoid valve are analyzed, and the dynamic simulation analysis of the opening process of the steam-operated solenoid valve is carried out based on Matlab/Simulink simulation software. The effects of valve core mass, spring stiffness, and spring preload on opening characteristics were obtained. A larger valve core mass results in longer opening and closing times for the moving iron core; a larger spring stiffness results in a longer opening time and a shorter closing time for the moving iron core. When the steam-operated solenoid valve opens, the response time increases as the spring preload force increases. When closing, the spring force assists in the resetting of the iron core, shortening the core reset time.

(3) Based on simulation results of static and dynamic characteristics, and combined with approximate models and experimental design methods, the structural parameters of the steam-operated solenoid valve were optimized. Regression model equations for the pull-in and release response times were established. Response surface methodology analysis showed that the interactions between different factors affecting the pull-in and release response times exhibited good linear relationships, leading to the acquisition of the optimal combination of structural parameters for the solenoid valve: *A* working air gap 2.1mm, *B* coil turns 3375, *C* valve core mass 99g, *D* spring stiffness 450N/m, and *E* spring preload 26N. This combination improved the solenoid valve's response time, yielding pull-in response time R_1 and release response time R_2 of 11.714ms and 9.122ms, respectively. The optimized scheme was ultimately selected, further enhancing the response speed.

This research improves the response characteristics of steam-operated solenoid valves, providing theoretical guidance for the design and optimization of solenoid valves with strong electromagnetic force and high dynamic response. It also has significance for improving the stability and reliability of solenoid valves under extreme operating conditions, expanding their application scope in engineering.

Declaration of competing interest

The authors declare that they have no known competing financial interests or

personal relationships that could have appeared to influence the work reported in this paper.

Acknowledgement

This research was funded by The Double First-Class Key Program of Gansu Provincial Department of Education, and Gansu Province Science and Technology Program Funding (Grant No. 22CX8GA125). Gansu Provincial Department of Education (Industrial Support Plan Project: 2025CYZC-048)

References

[1] Varganova A V, Khramshin V R, Radionov A A. Operating modes optimization for the boiler units of industrial steam plants[J]. Energies, 2023,16(6): 2596. https://doi.org/10.3390/en16062596

[2] Xie F, Zhou R, Wang D, et al. Simulation study on static and dynamic characteristics of electromagnet for electro-hydraulic proportional valve used in shock absorber[J]. IEEE Access, 2020,8:41870-41881. Doi: 10.1109/ACCESS.2020.2976713

[3] Hung N B, Lim O. Improvement of electromagnetic force and dynamic response of a solenoid injector based on the effects of key parameters[J]. International Journal of Automotive Technology, 2019,20:949-960. Doi: 10.1007/s12239–019–0089–5

[4] Gao H, Zhang F, Wang S, et al. Effect of characteristic parameters on the magnetic properties of voice coil motor for direct fuel injection in gasoline engine[J]. Energy Procedia, 2019,158:4184-4189. https://doi.org/10.1016/j.egypro.2019.01.811

[5] Feng Y, Xu T, Dai Y. Dynamic optimization method of high-speed solenoid valve parameters[C]//Journal of Physics: Conference Series. IOP Publishing, 2022,2296(1):012001. Doi: 10.1088/1742-6596/2296/1/012001

[6] Wang S, Weng Z, Jin B. A performance improvement strategy for solenoid electromagnetic actuator in servo proportional valve[J]. Applied Sciences, 2020,10(12):4352. https://doi.org/10.3390/app10124352

[7] REN Y, XI J, CHEN H, et al. Analysis of thermal effect on proportional solenoid valve used in vehicles based on hybrid modeling[J]. Transactions of Beijing institute of Technology, 2022,42(3):251-260. https://dx.doi.org/10.15918/j.tbit1001-0645.2021.057

[8] Zhang J, Liu P, Fan L, et al. Analysis on dynamic response characteristics of high-speed solenoid valve for electronic control fuel injection system[J]. Mathematical Problems in Engineering, 2020,2020(1):2803545. https://doi.org/10.1155/2020/2803545

[9] Cao D, Zhao W, Ji J, et al. Parametric equivalent magnetic network modeli ng approach for multiobjective optimization of PM machine[J]. IEEE Trans actions on Industrial Electronics, 2020,68(8):6619-6629. https://doi.org/10.110 9/TIE.2020.3005105

[10] Liu P, Fan L, Hayat Q, et al. Research on Key Factors and Their Interact ion Effects of Electromagnetic Force of High-Speed Solenoid Valve[J]. The scientific world journal, 2014,2014(1):567242. https://doi.org/10.1155/2014/5 67242

[11] Bhattacharyya B. Uncertainty quantification of dynamical systems by a PO D–Kriging surrogate model[J]. Journal of Computational Science, 2022,60:1 01602. https://doi.org/10.1016/j.jocs.2022.101602

[12] Wang B, Xie B, Xuan J, et al. AI-based optimization of PEM fuel cell ca talyst layers for maximum power density via data-driven surrogate modelin g[J]. Energy Conversion and Management, 2020,205:112460. https://doi.org/ 10.1016/j.enconman.2019.112460

[13] Liu P, Quan W, Wang J, et al. Static Performance Analysis and Optimizati on of High-Speed Solenoids Integrated with Permanent Magnets and Annul ar Flanges[C]//Actuators. MDPI, 2026, 15(3): 172. https://doi.org/10.3390/act 15030172

[14] Yu Z, Zhao J, Wei R. Multi-objective cooperation optimization research on dynamic response and energy loss of high-speed solenoid valve for diesel engine injector[J]. International Journal of Applied Electromagnetics and M echanics, 2024, 74(1): 57-77. https://doi.org/10.3233/JAE-230099

[15] Shen D F, Hao Z M, Zhao G, et al. Multi-objective optimization design o f solenoid valve based on BP neural network[J]. Journal of Xi'an Polytech nic University, 2023,37(2):79-86. Doi: 10.13338/j.issn.1674-649x.2023.02.011

[16] Guo D, Wang X, Gao K, et al. Evolutionary optimization of high-dimensi onal multiobjective and many-objective expensive problems assisted by a d ropout neural network[J]. IEEE transactions on systems, man, and cyberneti cs: systems, 2021,52(4):2084-2097. https://doi.org/10.1109/TSMC.2020.30444

[17] Dong H, Li J, Wang P, et al. Surrogate-guided multi-objective optimization (SGMOO) using an efficient online sampling strategy[J]. Knowledge-Based Systems, 2021,220:106919. https://doi.org/10.1016/j.knosys.2021.106919

[18] Karidis J P, Turns S R. Optimization of Electromagnetic Actuator Perform ance for High-Speed Valves[J]. 1986. https://doi.org/10.1115/1.3258739

[19] Feng X, Liu Z, Tian Z, et al. Interaction of structural parameters and mul ti-objective optimization of dynamic response characteristics in dual-fuel inj ectors[J]. Applied Thermal Engineering, 2026:131056. https://doi.org/10.1016 /j.applthermaleng.2026.131056

[20] Chen D C, Chen L R. Application of the Taguchi method for finite eleme nt analysis of a shear-type magnetorheological fluid damper[J]. Advances i n Mechanical Engineering, 2020,12(4):1687814019900397. https://doi.org/10. 1177/1687814019900397

[21] Fan X, Zhu Y. Collaborative optimization of multi-physical fields for comp osite electromagnetic linear actuators[J]. International Journal of Applied El ectromagnetics and Mechanics, 2024,76(3):306-322. https://doi.org/10.3233/J AE-230428

[22] Meng X, Li Y, Ni X, et al. Optimization design and analysis of the propo rtional solenoid valve for the power shift transmission of cotton picker usi ng NSGA-II algorithm[J]. International Journal of Agricultural and Biologic al Engineering, 2026, 19(2): 158-169. Doi: 10.25165/j.ijabe.20261902.10167

[23] Zhang X, Lu Y, Li Y, et al. Numerical calculation and experimental study on response characteristics of pneumatic solenoid valves[J]. Measurement a nd control, 2019, 52(9-10): 1382-1393. https://doi.org/10.1177/002029401986 6853

[24] Li T, Zhang Y, Liang Y, et al. Multiobjective optimization research on the response time of a pneumatic pilot-operated high speed on/off valve[J]. In ternational Journal of Applied Electromagnetics and Mechanics, 2021,65(1): 109-127. https://doi.org/10.3233/JAE-190074

[25] Jiang H W. Simulation Analysis and Experimental Test on Opening Characteristics of High-Pressure Solenoid Valves[D]. Southwest University of Science and Technology, 2023. Doi: 10.27415/d.cnki.gxngc.2023.000418

[26] Yang J C. Design and Performance Research of Solenoid Valve for Electronic Controlled Injector of Marine High-Power High-Speed Diesel Engine [D]. Huazhong University of Science and Technology, 2021. Doi: 10.27157/d.cnki.ghzku.2021.001354

[27] Zong S Y. Research on Key Performance of High-Speed On-Off Valves[D]. Wuhan University of Technology, 2020. Doi: 10.27381/d.cnki.gwlgu.2020.001362

[28] Wan L P. Research on Solenoid Valve Performance in Braking System[D]. South China University of Technology, 2021. Doi: 10.27151/d.cnki.ghnlu.2021.000259

[29] Xue J. Study on Static and Dynamic Characteristics and Interaction Mechanism of Vehicle Solenoid Valve[D]. Hunan University of Science and Technology, 2023. Doi: 10.27738/d.cnki.ghnkd.2023.001268

[30] Liu Y, Hu Y, Zhu N, et al. A decomposition-based multiobjective evolutionary algorithm with weights updated adaptively[J]. Information Sciences, 2021,572: 343-377. https://doi.org/10.1016/j.ins.2021.03.067

[31] Yu Z, Wei S, Wu C, et al. Development and verification of RP-3 aviation kerosene surrogate fuel models using a genetic algorithm[J]. Fuel, 2022,312:122853. https://doi.org/10.1016/j.fuel.2021.122853

DATA AVAILABILITY

The datasets used and/or analysed during the current study are available from the corresponding author on reasonable request